DOI: 10.1002/ejic.200701369

Bioinspired Energy Conversion Systems for Hydrogen Production and Storage

Shunichi Fukuzumi*[a]

Keywords: Artificial photosynthesis / Photoinduced electron transfer / Hydrogen production / Hydrogen storage / Sustainable chemistry

Recent developments in photocatalytic hydrogen production by using artificial photosynthesis systems is described, together with those in hydrogen storage through the fixation of CO_2 with H_2. Hydrogen can be stored in the form of formic acid, which can be converted back to H_2 in the presence of an appropriate catalyst. Electron donor–acceptor dyads are utilized as efficient photocatalysts to reduce methyl viologen (MV^{2+}) by NADH (β-nicotinamide adenine dinucleotide, reduced form) analogues to produce the methyl violgen radical cation that acts as an electron mediator for the production of hydrogen. Porphyrin-monolayer-protected gold clusters that enhance the light harvesting efficiency can also be used for the photocatalytic reduction of methyl viologen by NADH analogues. The use of a simple electron donor–acceptor dyad, the 9-mesityl-10-methylacridinium ion (Acr^+–Mes), enables the construction of a highly efficient photocatalytic hydrogen-evolution system without an electron mediator such as MV^{2+}, with poly(*N*-vinyl-2-pyrrolidone)-protected platinum nanoclusters (Pt–PVP) and NADH as a hydrogen-evolution catalyst and an electron donor, respectively. Hydrogen thus produced can be stored in the form of formic acid (liquid) by fixation of CO_2 with H_2 in water by using ruthenium aqua complexes $[Ru^{II}(\eta^6\text{-}C_6Me_6)(L)(OH_2)]^{2+}$ [L = 2,2′-bipyridine (bpy), 4,4′-dimethoxy-2,2′-bipyridine (4,4′-OMe-bpy)] and iridium aqua complexes $[Ir^{III}Cp^*(L)(OH_2)]^{2+}$ ($Cp^* = \eta^5\text{-}C_5Me_5$, L = bpy, 4,4′-OMe-bpy) as catalysts at pH 3.0. Catalytic systems for the decomposition of HCOOH to H_2 are also described. The combination of photocatalytic hydrogen generation with the catalytic fixation of CO_2 with H_2 and the decomposition of HCOOH back to H_2 provides an excellent system for cutting CO_2 emission.

Introduction

The rapid consumption of fossil fuel has caused unacceptable environmental problems such as the greenhouse effect by CO_2 emission, which could lead to disastrous climatic consequences.[1,2] The consumption rate is expected to increase further by at least a factor of two by the middle of the century because of population and economic growth, particularly in the developing countries. Thus, renewable and clean energy resources are required in order to solve global energy and environmental issues. Among renewable energy resources, solar energy is by far the largest exploitable resource.[2]

Hydrogen is a clean energy source for the future and can be used to reduce the dependence on fossil fuels and the emissions of greenhouse gases in the long-term.[3] Should greenhouse warming turn out to be an important problem, the key advantage of hydrogen is that carbon dioxide is not produced when hydrogen is burned to produce only water. Hydrogen should be produced, ideally by splitting water (H_2O), by using solar energy. Hydrogen storage is also a key enabling technology for the advancement of hydrogen and fuel cell power technologies in transportation, stationary, and portable applications.[4]

The development of artificial photosynthesis systems by using a large portion of the solar spectrum would be a

[a] Department of Material and Life Science, Graduate School of Engineering, Osaka University, SORST, Japan Science and Technology Agency,
2-1 Yamada-oka, Suita, Osaka 565-0871, Japan
Fax: +81-6-6879-7370
E-mail: fukuzumi@chem.eng.osaka-u.ac.jp

Shunichi Fukuzumi earned a bachelor's degree and a PhD degree in applied chemistry at Tokyo Institute of Technology in 1973 and 1978, respectively. After working as a postdoctoral fellow (1978–1981) at Indiana University in USA, he joined the Department of Applied Chemistry, Osaka University, as an Assistant Professor in 1981 and was promoted to a Full Professor in 1994. His research interests lie in electron transfer in all fields of chemistry. He has been the director of a CREST (Core Research for Evolutional Science and Technology) project of the Japan Science and Technology Agency since 1999, which is now extended as a SORST (Solution Oriented Research for Science and Technology) project. He is currently the leader of a Global COE program, Global Education and Research Center for Bio-Environmental Chemistry that started in 2007.

major advance in energy production and a critical breakthrough with respect to the rising concern of environmental pollution caused by the use of conventional fossil fuels.[2] The design of such systems can be guided by the key steps of natural photosynthesis, such as the efficient capture of visible light photons and electron/hole separation through electron transfer to give energetic oxidizing and reducing equivalents with long lifetimes (≈1 s).[5] However, even a relatively simple bacterial photosynthesis system is extremely complex, and its synthetic imitation has been a challenging task.

Mimicking of the natural photosynthesis process requires synthetic models of all the important components and the linking of these models together into a working molecular assembly. There have been a number of excellent reviews on electron donor–acceptor ensembles as synthetic models mimicking charge-separation processes in the photosynthesis reaction center.[6–18]

In this review, recent developments in photocatalytic hydrogen production is described, with a focus on the combination of synthetic models of charge-separation processes in the photosynthesis reaction center and catalysts for hydrogen evolution. A proposal for the storage of hydrogen is also described in relation with the important issue of the reduction in CO_2 emission.

Photocatalytic Hydrogen Evolution with Electron Mediators

A large number of photocatalytic hydrogen-evolution systems have been developed in the past decades.[19–34] Such systems usually consist of an electron donor, a photosensitizer, an electron mediator such as methyl viologen (MV^{2+}), and a hydrogen-evolution catalyst such as Pt nanoclusters (Scheme 1). Photosensitizers have been linked covalently or noncovalently with MV^{2+} in order to improve the charge-separation efficiency in the hydrogen-evolution photocatalytic system.[31–34] However, the lifetime of the charge-separated state is relatively short, and the catalytic activity of hydrogen production with $MV^{\bullet+}$ is also low, and it therefore takes a long time (e.g. hours) to obtain an appreciable amount of hydrogen.

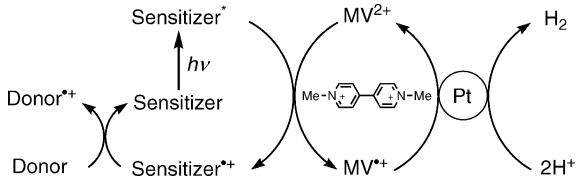

Scheme 1. Conventional photocatalytic systems for hydrogen evolution with an electron mediator (methyl viologen).

In order to attain long-lived charge-separated (CS) states, extensive efforts have so far been devoted to develop electron donor–acceptor linked systems that can be used in the mimicking of photoinduced electron-transfer processes in the natural photosynthesis reaction center.[6–18] Electron donor–acceptor ensembles such as zinc porphyrin-C_{60} (ZnP-C_{60})[35] and the zinc porphyrin-free base porphyrin-fullerene triad (ZnP-H_2P-C_{60})[35] have been shown to act as efficient photocatalysts for the uphill oxidation of an NADH analogue, 1-benzyl-1,4-dihydronicotineamide (BNAH),[36] by hexyl viologen (HV^{2+}), as shown in Scheme 2.[37] Electron transfer from BNAH to $ZnP^{\bullet+}$ is exothermic, considering the one-electron oxidation potential of BNAH (E_{ox} = 0.57 V vs. SCE),[36] which is 0.14 V less positive than the reduction potential of $ZnP^{\bullet+}$ (0.71 V vs. SCE).[35] Electron transfer from $C_{60}^{\bullet-}$ (E_{ox} = –0.67 V vs. SCE)[35] to HV^{2+} (E_{red} = –0.42 V vs. SCE)[37] is also exothermic. Thus, once the CS state is obtained by photoirradiation of ZnP-C_{60}, the oxidation of BNAH and the reduction of HV^{2+} are accomplished by electron transfer with $ZnP^{\bullet+}$ and $C_{60}^{\bullet-}$, respectively (Scheme 2).[37] The occurrence of such an electron transfer was confirmed by laser flash photolysis measurements.[37] Thus, both ZnP-C_{60} and ZnP-H_2P-C_{60} donor–acceptor ensembles act as efficient photocatalysts for the uphill oxidation of NADH analogues by HV^{2+} in benzonitrile. In the case of ZnP-C_{60}, the quantum yield of the photocatalytic reaction increases with increasing concentration of HV^{2+} or BNAH, to reach a limiting value of 0.99.[37] The limiting quantum yields of ZnP-C_{60} and ZnP-H_2P-C_{60} agree well with the quantum yields of the CS states $ZnP^{\bullet+}$-$C_{60}^{\bullet-}$ and $ZnP^{\bullet+}$-H_2P-$C_{60}^{\bullet-}$, respectively.[35] The longer lifetime of the $ZnP^{\bullet+}$-spacer-$C_{60}^{\bullet-}$ state in the triad (8.3 μs) relative to that of the dyad (0.8 μs) results in facilitated redox reactions involving the CS state, BNAH and HV^{2+}.[37] A different NADH analogue (10-methyl-9,10-dihydroacridine) can also be used as an electron source.[37]

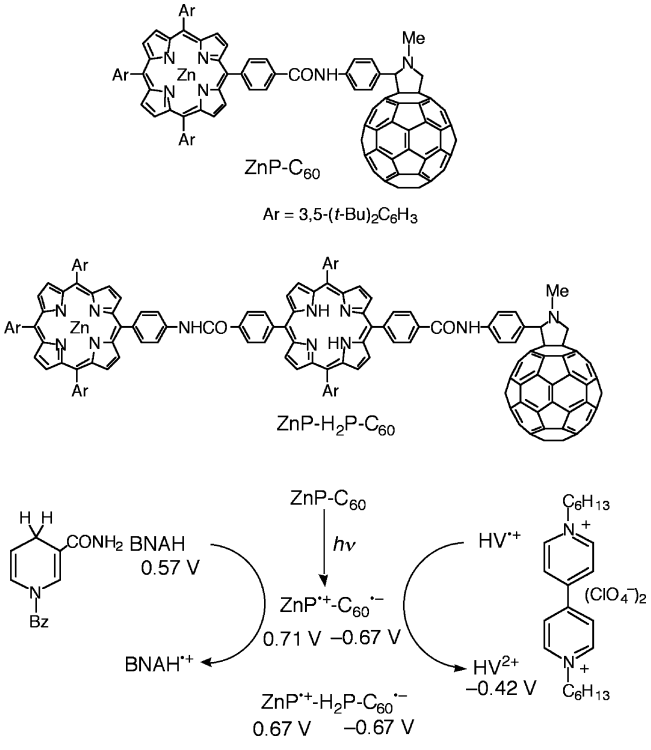

Scheme 2. Photocatalytic reduction of hexyl viologen (HV^{2+}) by an NADH analogue (BNAH) with an electron donor–acceptor dyad (ZnP-C_{60}) and triad (ZnP-H_2P-C_{60}).[37]

The light-harvesting efficiency has been significantly enhanced by the construction of three-dimensional architectures of monolayer-protected gold nanoclusters with porphyrins (H_2PCnAuMPC), as shown in Figure 1a.[38] H_2PCnAuMPC was prepared by reduction of $AuCl_4^-$ with $NaBH_4$ in toluene containing bis(porphyrin) disulfide.[38] The mean diameter of the gold core determined by TEM (Figure 1b) was 2.4 ± 0.6 nm.[38] The interaction of the porphyrin excited state with the gold nanocluster is reduced significantly, relative to the bulk gold surface, because of the "quantum effect",[39,40] which enables the development of a new type of light-harvesting materials.[38]

The photocatalytic function of the three-dimensional porphyrin monolayer-protected gold nanoclusters (MPCs) with different chain lengths (H_2PCnAuMPC: n = 3, 11) has been examined in the reduction of HV^{2+} by BNAH and compared with that of the reference porphyrin compound without metal nanoclusters.[41] The fluorescence lifetime (60 ps) of H_2PC_3AuMPC is shorter than that of $H_2PC_{11}AuMPC$ (130 ps) because of the faster energy transfer from $^1H_2P^*$ to the gold nanocluster with the shorter chain length.[41] In such a case, $H_2PC_{11}AuMPC$ acts as a more efficient photocatalyst than H_2PC_3AuMPC and the reference porphyrin for the uphill reduction of HV^{2+} by BNAH to produce BNA^+ and $HV^{\cdot+}$ in benzonitrile.[41] The quantum yield reaches a maximum value at an extremely small concentration of HV^{2+}, which is significantly larger than the corresponding value for the reference porphyrin compound.[41] The three-dimensional architectures of porphyrin MPCs with a large surface area allow the interaction of HV^{2+} with the MPCs to form the supramolecular complex, which results in fast electron transfer from the singlet excited state of the porphyrin to HV^{2+} on the MPCs (Scheme 3).[41] This is the reason why the quantum yield for the photocatalytic reduction of HV^{2+} by BNAH reaches a maximum value at an extremely small concentration of HV^{2+} when the surface of MPCs is covered by HV^{2+}. BNAH is oxidized by the resulting $H_2P^{\cdot+}$ to produce $BNAH^{\cdot+}$ and is accompanied by the regeneration of H_2PC11AuMPC. The subsequent step is the deprotonation of $BNAH^{\cdot+}$,[36] followed by electron transfer from $BNA^{\cdot}$ to HV^{2+} (Scheme 3).[41] Thus, the light-harvesting efficiency of the MPCs is significantly better than that of the reference compound.

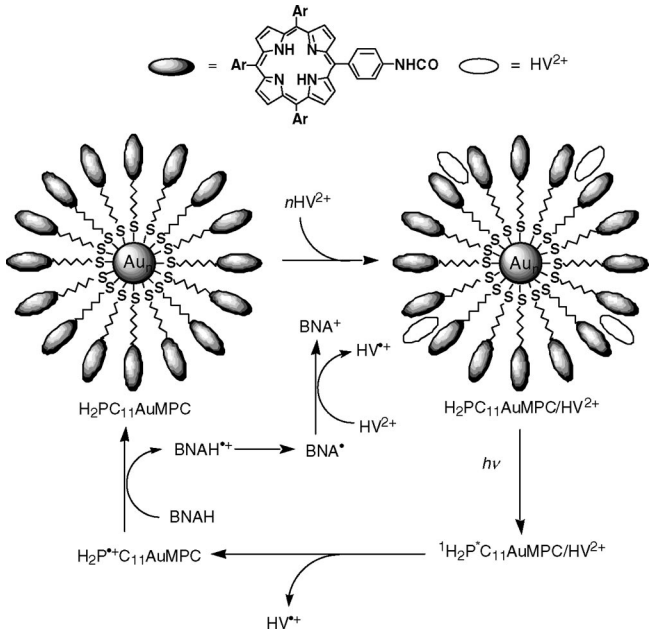

Scheme 3. Photocatalytic reduction of hexyl viologen (HV^{2+}) by an NADH analogue (BNAH) with the porphyrin monolayer-protected gold nanocluster (H_2PC11AuMPC) through the formation of the supramolecular complex between H_2PC11AuMPC and HV^{2+}.[41]

Once the viologen radical cation is formed, electron transfer from the viologen radical cation to the platinum nanoclusters results in the evolution of hydrogen by using H^+. The catalytic efficiency of hydrogen evolution is improved significantly by using water-soluble platinum nanoclusters functionalized with methyl viologen-alkanethiol

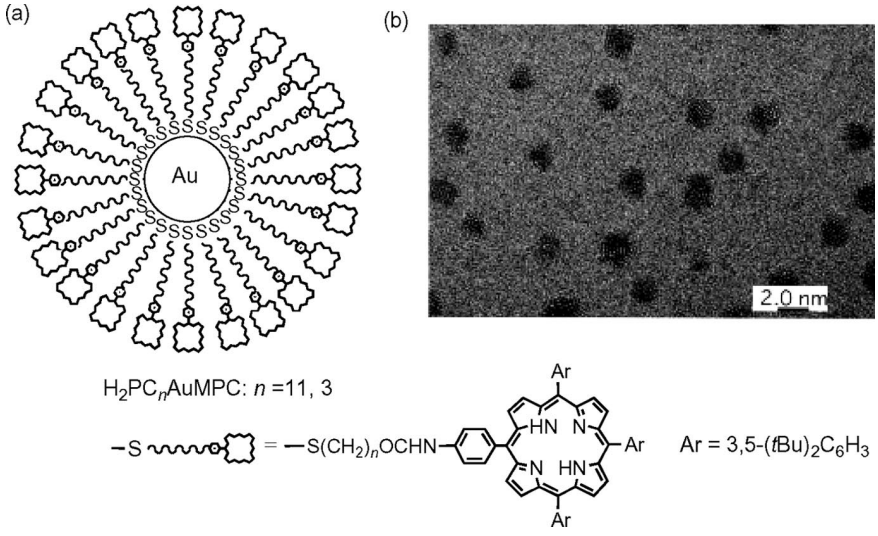

Figure 1. Porphyrin monolayer-protected gold nanocluster (H_2PCnAuMPC) and the TEM image (n = 11).[38]

(MVA^{2+}).[42] The methyl viologen-modified platinum nanoclusters (MVA^{2+}–PtC) were prepared by applying the same method used for the preparation of alkanethiolate-modified gold nanoparticles,[43,44] i.e. reduction of H_2PtCl_6 with $NaBH_4$ in water containing MVA^{2+} (MVA^{2+}/H_2PtCl_6 = 1:1), as shown in Scheme 4.[42] The mean diameter of the platinum core (2RCORE) was determined by transmission electron microscopy (TEM) as 1.9 nm range,[42] which is similar to the diameter reported for the water-soluble platinum nanoclusters.[45,46] MVA^{2+}–PtC with a diameter of 1.9 nm comprises 210 platinum atoms, of which 130 lie on the Pt surface. The number of MVA^{2+} species on the Pt surface is determined as 67 from the elemental analysis of MVA^{2+}–PtC.[42]

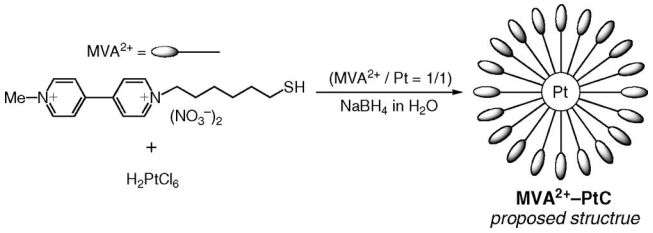

Scheme 4. Synthetic procedure for methyl viologen-modified platinum nanoclusters (MVA^{2+}–PtC).[42]

The photocatalytic system for hydrogen evolution with NADH as a sacrificial agent in an aqueous solution (Scheme 5)[42] has been constructed by using MVA^{2+}–PtC and a simple electron–donor dyad, 9-mesityl-10-methylacridinium ion (Acr^+–Mes), which is capable of fast photoinduced electron transfer, but extremely slow back electron transfer.[47,48] As a result, the rate of evolution of hydrogen for the photocatalytic system with MVA^{2+}–PtC is 10 times faster than that for the photocatalytic system with a mixture of the same amount of MVA^{2+} and platinum clusters as that in MVA^{2+}–PtC under the same experimental conditions.[42]

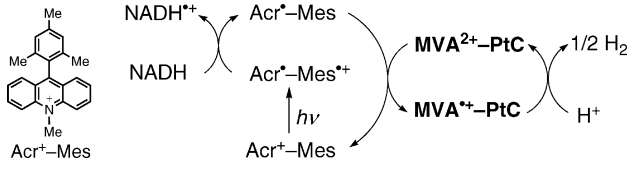

Scheme 5. Phocatalytic scheme for the evolution of hydrogen with NADH by using Acr^+–Mes and MVA^{2+}–PtC as the photocatalyst and proton reduction catalyst, respectively.[42]

First, the photoirradiation of Acr^+–Mes results in formation of the electron-transfer state ($Acr^{\cdot}$–$Mes^{\cdot+}$).[47–49] The electron-transfer oxidation of NADH and the electron-transfer reduction of MVA^{2+} in MVA^{2+}–PtC then occur with $Acr^{\cdot}$–$Mes^{\cdot+}$. Both processes are thermodynamically feasible, because the one-electron oxidation potential of NADH (E_{ox} = 0.76 V vs. SCE)[50,51] is less positive than the one-electron reduction potential of the $Mes^{\cdot+}$ moiety of $Acr^{\cdot}$–$Mes^{\cdot+}$ (E_{red} = 1.88 V vs. SCE)[47] and the one-electron oxidation potential of the $Acr^{\cdot}$ moiety (E_{ox} = –0.57 V vs. SCE)[47] of $Acr^{\cdot}$–$Mes^{\cdot+}$ is more negative than the one-electron reduction potential of the MVA^{2+} moiety in MVA^{2+}–PtC (E_{red} = –0.50 V).[42] In contrast, however, electron transfer from $Acr^{\cdot}$–$Mes^{\cdot+}$ (E_{ox} = –0.57 V vs. SCE) to MV^{2+} (E_{red} = –0.67 V) is energetically unfavorable because the E_{ox} value of $Acr^{\cdot}$–$Mes^{\cdot+}$ is more positive than the E_{red} value of MV^{2+}.[42] In such a case, MV^{2+} may be reduced by $NAD^{\cdot}$, which is produced by deprotonation of $NADH^{\cdot+}$, since the electron transfer from $NAD^{\cdot}$ (E_{ox} = –1.1 V vs. SCE)[50,51] to MV^{2+} (E_{red} = –0.67 V) is highly exergonic. Thus, $Acr^{\cdot}$–$Mes^{\cdot+}$ is more efficiently quenched in the NADH/MVA^{2+}–PtC system than in the NADH/MV^{2+}/Pt–PVP system. In addition, the electron transfer from $MVA^{\cdot+}$ to the Pt clusters is certainly more efficient in the MVA^{2+}-bound Pt clusters relative to the intermolecular electron transfer from $MV^{\cdot+}$ to Pt–PVP in solution, which leads to the 10 times faster H_2 evolution rate.[42]

Photocatalytic Hydrogen Evolution without Electron Mediators

As described above, an electron mediator such as MV^{2+} is believed to be required in the photocatalytic hydrogen-evolution system (Scheme 1). However, a highly efficient photocatalytic hydrogen-evolution system *without an electron mediator*, composed of Acr^+–Mes, NADH, and a water-soluble platinum colloid, has been constructed to achieve the highest quantum yield for hydrogen production ($26 \pm 3\%$) ever reported.[52] Photoirradiation ($\lambda > 390$ nm) of a deaerated phthalic acid buffer (pH 4.5, 50 mM) and MeCN [1:1 (v/v)] mixed solution (2.0 cm^3) containing Acr^+–Mes (0.10 mM), NADH (1.0 mM), and Pt–PVP (0.20 mg) results in the highly efficient evolution of hydrogen.[52] Figure 2 shows the dependence of the amount of hydrogen evolved on the irradiation time in the absence (●) and presence (○) of MV^{2+}.[52] The hydrogen-evolution rate in the absence of MV^{2+} was determined as 14.7 μmol h^{-1} from the slope of Figure 2, which is 300 times faster than that with MV^{2+} (0.05 μmol h^{-1}). This indicates that MV^{2+} acts as an inhibitor in this photocatalytic hydrogen-evolution system.

The significant retarding effect of MV^{2+} on the photocatalytic evolution of hydrogen seen in Figure 2 is attributed to efficient electron transfer from $Acr^{\cdot}$–Mes to MV^{2+}, which results in the formation of $MV^{\cdot+}$. This latter species is much less reactive than $Acr^{\cdot}$–Mes for the reduction of Pt–PVP to produce hydrogen. The rate of electron-transfer reduction of Pt–PVP by $Acr^{\cdot}$–Mes is much faster than that by $MV^{\cdot+}$.[52] Under the same experimental conditions as that for Figure 2 (generated hydrogen was analyzed 1 min after photoirradiation), $MV^{\cdot+}$ remained in the resulting solution because of slow electron transfer from $MV^{\cdot+}$ to Pt–PVP, whereas no $Acr^{\cdot}$–Mes remained without MV^{2+} because of the much faster electron transfer from $Acr^{\cdot}$–Mes to Pt–PVP. Such a difference in the electron-transfer reactivity between $Acr^{\cdot}$–Mes and $MV^{\cdot+}$ may result from the absence of electro-

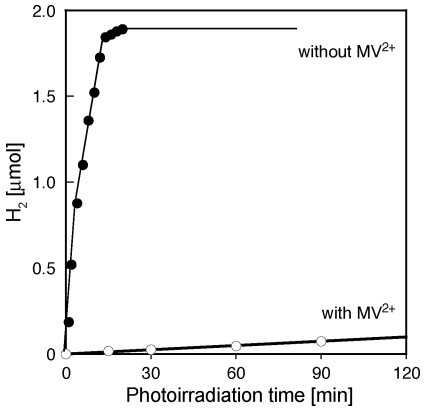

Figure 2. Dependence of evoltuion of hydrogen on the irradiation time under steady-state irradiation ($\lambda > 390$ nm) of a deaerated phthalic acid buffer (pH 4.5, 50 mM) and MeCN [1:1 (v/v)] mixed solution (2.0 cm^3) containing Acr^+–Mes (0.10 mmol dm^{-3}), NADH (1.0 mmol dm^{-3}), and Pt–PVP (0.20 mg) in the absence (●) and presence (○) of MV^{2+} (5.0 mM) at 298 K.[52]

static repulsion between the neutral electron donor (Acr•–Mes) and Pt–PVP with the positive charge on the Pt surface,[53,54] in contrast with the positively charged electron donor ($MV^{•+}$). The rate constant of the electron-transfer reduction of Pt–PVP by Acr•–Mes increases linearly with decreasing pH (pH 4.5–5.9).[52] This indicates that proton-coupled electron transfer from Acr•–Mes to Pt–PVP is the rate-determining step in the catalytic evolution of hydrogen. The active site of Pt–PVP may be Pt^{II}–PVP on the surface, which can be reduced by Acr•–Mes in the presence of H^+ to produce a Pt–H intermediate.

The laser photoirradiation of Acr^+–Mes with NADH results in electron transfer from NADH to Acr•–$Mes^{•+}$ to produce the NADH radical cation ($NADH^{•+}$) and Acr•–Mes. The formation of Acr•–Mes is clearly seen as the transient absorption band at λ_{max} = 520 nm. The transient absorption due to $NADH^{•+}$ is not seen, but instead the initial bleaching at 420 nm increases and is accompanied by an increase in the intensity of the absorption band at 520 nm assigned to Acr•–Mes. This indicates that additional Acr•–Mes is formed by electron transfer from NAD•, which is formed by rapid deprotonation of $NADH^{•+}$, to Acr^+–Mes as shown in Scheme 6. The increase in bleaching results from a decrease in the intensity of the absorption band at 420 nm assigned to NAD•. As a result, 2 equiv. Acr•–Mes are produced by 1 equiv. NADH that acts as a two-electron donor. The quantum yield for the formation of Acr•–Mes was determined to be 0.52 from the absorbance band at 520 nm assigned to the Acr• moiety.[52]

The total quantum yield for the evolution of hydrogen (Φ) was then determined by comparing the amount of hydrogen evolved with that of Acr•–Mes.[52] Figure 3 shows that the amount of hydrogen is half that of Acr•–Mes.[52] As a result, the value of Φ was determined to be 0.26 ± 0.03% by comparison with the quantum yield of Acr•–Mes (0.52).[52]

NADH used as an electron source can be replaced by ethanol, because ethanol can reduce NAD^+ to regenerate

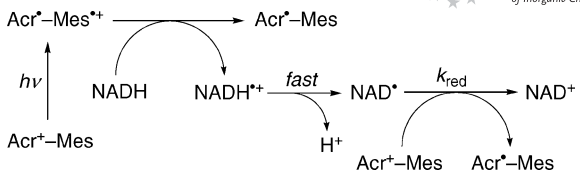

Scheme 6. Photooxidation mechanism of NADH following the photoexcitation of Acr^+–Mes.[52]

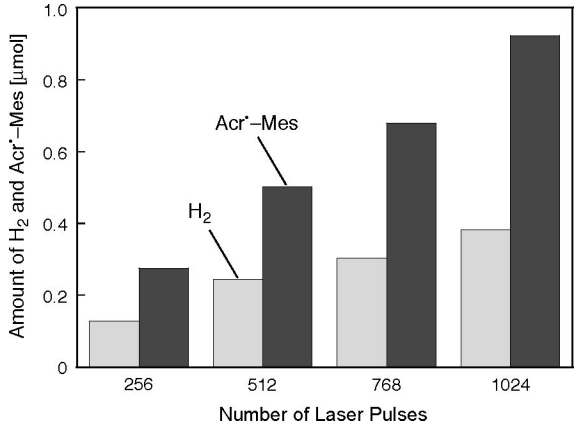

Figure 3. Comparison of the amount of evolved hydrogen and of Acr•–Mes after laser excitation (λ = 430 nm) of a deaerated phthalic acid buffer (pH 4.5, 50 mM) and MeCN [1:1 (v/v)] mixed solution (2.0 cm^3) containing Acr^+–Mes (0.10 mM) and NADH (2.0 mM) at 298 K.[52]

NADH in the presence of alcohol dehydrogenases (ADH).[55] Photoirradiation ($\lambda > 390$ nm) of a deaerated phosphate buffer solution containing ethanol, Acr^+–Mes, ADH, NAD^+, and Pt–PVP results in the formation of hydrogen from ethanol (Scheme 7).[52]

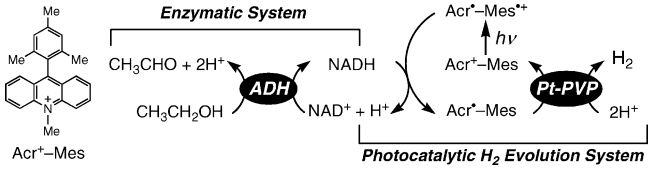

Scheme 7. Phocatalytic scheme for the evolution of hydrogen from ethanol with Acr^+–Mes, ADH, NAD^+, and Pt–PVP.[52]

A photocatalytic hydrogen evolution system without an electron mediator was also made by using a "molecular device" composed of a bis(2,2′-bipyridine)ruthenium(II) derivative and a dichloro(2,2′-bipyridine)platinum(II) derivative, $[RuPt]^{2+}$, in the presence of a sacrificial electron donor (EDTA) in water under illumination by visible-light.[56] $[RuPt]^{2+}$ was prepared by 1:1 condensation of $[Ru–NH_2]^{2+}$ ($[Ru(5\text{-aminophen})(bpy)_2]^{2+}$;[57] phen = 1,10-phenanthroline, bpy = 2,2′-bipyridine) and 4,4′-bis(chlorocarbonyl)-2,2′-bipyridine, which first afforded a complex li-

gand [Ru–bpy]$^{2+}$ (Scheme 8).[56] The chloride salt of this complex reacts with K_2PtCl_4 in water to give [RuPt]$^{2+}$ (Scheme 8).[56] The [RuPt]$^{2+}$ complex is effective in the visible-light-induced EDTA-reduction of water to H_2, although the quantum yield is rather low (Φ = 1%).[56]

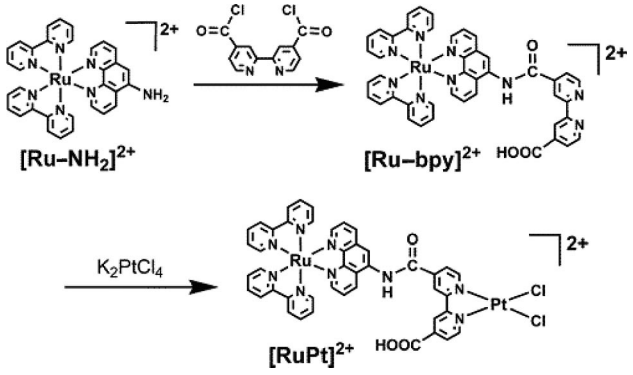

Scheme 8. Synthetic procedure for the preparation of a "molecular device" [RuPt]$^{2+}$ composed of the bis(2,2′-bipyridine)ruthenium(II) derivative [Ru–NH_2]$^{2+}$ and a dichloro(2,2′-bipyridine)platinum(II) derivative.[56]

The interfacing of nanostructured semiconductor photoelectrodes with redox proteins acting as light-absorbing chromophores (Scheme 9) has also provided an innovative approach to the development of photocatalytic hydrogen-evolution systems.[58] The photoinduced electron transfer from zinc-substituted cytochrome *c*, ZnCyt-*c*, immobilized on mesoporous, nanocrystalline metal oxide electrodes occurs by the transfer of an electron from the triplet state of ZnCyt-*c* to the TiO_2 electrodes. This results in a long-lived CS state (lifetime of up to 0.4 s). The optimum yield of a long-lived CS state was obtained by employing TiO_2 electrodes at pH 5. The addition of EDTA as a sacrificial electron donor to the electrolyte resulted in efficient photogeneration of H_2 with a quantum yield per absorbed photon of 10 ± 5%.[58] This value is higher than that reported previously for analogous dye-sensitized nanocrystalline TiO_2 photoelectrodes.[59,60] The high efficiency may result from the long lifetime (0.4 s) of the $TiO_2(e^-)$/ZnCyt-$c^{\cdot+}$ CS state, along with a reasonable CS quantum efficiency.

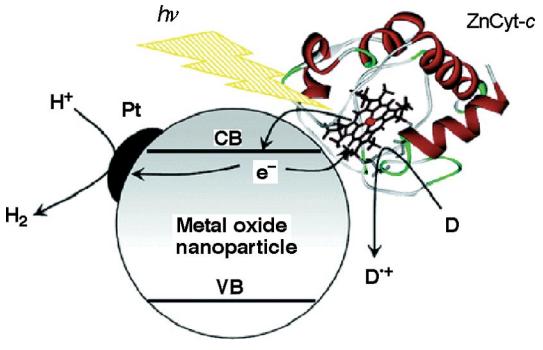

Scheme 9. Schematic representation of the ZnCyt-*c*/metal oxide based artificial photosystem.[58]

Alternatives to Pt Catalyst for H_2 Evolution

The hydrogen-evolution step described above is catalyzed most effectively by the Pt group metals. It would be preferable to replace those metals by metals that are cheap and abundant. In this context, hydrogenases have also been used instead of Pt nanoclusters as catalysts for photocatalytic hydrogen evolution.[29–32] Hydrogenase enzymes have merited considerable interest, because they can catalyze the hydrogen-evolution reaction and the reverse reaction at rapid rates at room temperature.[61,62] Hydrogenases contain metals that are less noble than Pt; [NiFe] hydrogenases represent the largest class of hydrogenases and contain an Ni and a Fe atom, whereas Fe-only hydrogenases contain one or two Fe atoms.[61–64] The efficient catalytic function of hydrogenases for hydrogen evolution and the increasing demand for a cheaper metal catalyst to replace the expensive Pt catalyst have fuelled intensive research aimed at the synthesis of close molecular mimics that can achieve a comparable catalytic activity.[65–67]

X-ray crystallographic studies have shown that the core structure of [NiFe] hydrogenase from *D. gigas* in the resting state consists of one nickel atom and one iron atom, which are bridged by two cysteic thiolates and one unidentified ligand (X), as shown in Figure 4.[68,69] The bridging ligand X in the resting state is believed to be an oxygen-containing ligand such as H_2O, OH^-, or O_2^{-}.[70] The active form is believed to be a [Ni(μ-H)Fe] species that may be produced by the heterolytic activation of H_2 with the resting form.[71] The first successful isolation and determination of a crystal structure of the molecular mimics of the active form of hydrogenases has been achieved for a [Ni(μ-H)Ru] complex, $[(OH_2)Ni^{II}(\mu\text{-}H)(L)Ru^{II}(\eta^6\text{-}C_6Me_6)](NO_3)$ [L = *N*,*N*′-dimethyl-*N*,*N*′-bis(2-mercaptoethyl)-1,3-propanediamine], which was synthesized from the reaction of a dinuclear [NiRu] aqua complex $[Ni^{II}(L)Ru^{II}(\eta^6\text{-}C_6Me_6)(OH_2)]](NO_3)_2$ with H_2 in water under ambient conditions (Scheme 10).[71]

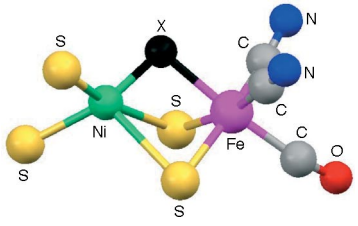

Figure 4. Core structure of the resting form of [NiFe] hydrogenase from *D. gigas* determined by X-ray analysis.[70]

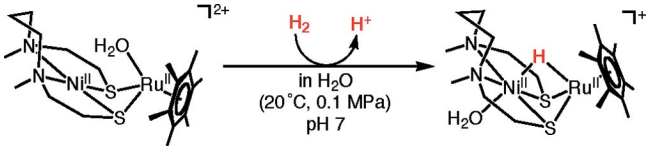

Scheme 10. Formation of a [Ni(μ-H)Ru] complex by the reaction of a dinuclear [NiRu] aqua complex with H_2.[71]

The X-ray analysis of the dinuclear [Ni(μ-H)Ru] complex indicates that the structure is similar to the core structure of the proposed active form of [NiFe] hydrogenase (Figure 5).[71] The metal ions and the bridging ligands cooperate to activate H_2 in water under ambient conditions. The geometry around the Ni^{II} ion changes from square planar for the [NiRu] aqua complex to distorted octahedral for the [Ni(μ-H)Ru] complex. The tunable Ni–S–Ru bite angles allow such a structural change in the dinuclear complex. The H_2O ligand of the [NiRu] aqua complex may play an important role in the activation of H_2 by accelerating the heterolytic cleavage by acting as a base.

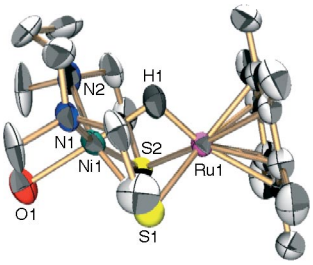

Figure 5. X-ray crystal structure of a [Ni(μ-H)Ru] complex, $[(OH_2)Ni^{II}(\mu\text{-}H)(L)Ru^{II}(\eta^6\text{-}C_6Me_6)]^+$ (L = *N*,*N*′-dimethyl-*N*,*N*′-bis(2-mercaptoethyl)-1,3-propanediamine).[71]

Nitrogenases are also effective catalysts for the hydrogen-evolution reaction.[72,73] The structure of the nitrogenase active site (Figure 6a)[74] and the MoS_2 edge structure (Figure 6b)[75] are similar, namely the sulfur atom, which binds hydrogen, is coordinated to two metal atoms, either to molybdenum or to iron. Only the edges of MoS_2 are important as the catalytic site, since the basal plane of MoS_2 is catalytically inactive.[76] A good material would be nanometer-sized MoS_2 crystallites supported on, for example, graphite, which is conducting but otherwise inert. Nanosized MoS_2 clusters on a graphite support were prepared and exhibit the catalytic activity for electrochemical hydrogen evolution.[75] Electrocatalytic activity for the evolution of hydrogen correlates linearly with the number of edges on the MoS_2 catalyst.[77] Further studies on molecular mimics of hydrogenases and nitrogenases are necessary for the development of more efficient catalysts for the hydrogen-evolution reaction.

H_2 Storage with CO_2

Hydrogen has attracted considerable attention recently with increasing interest as an environmentally acceptable, alternative energy carrier.[78,79] However, hydrogen is quite difficult to store or transport with current technology, because hydrogen gas has a poor energy density by volume relative to hydrocarbons, and it therefore requires a larger tank for storage purposes. By increasing the gas pressure the energy density by volume would improve, which would result in a smaller volume. However, the compression of hydrogen gas requires energy to power the compressor and also heavy container tanks. Thus, hydrogen storage is a significant challenge for the widespread use of hydrogen as a renewable fuel. Current approaches towards the storage of hydrogen include compressed hydrogen-gas tanks, liquid-hydrogen tanks, metal hydrides, carbon-based materials/high surface area sorbents, and chemical hydrogen storage. Low-cost, energy-efficient storage of hydrogen is definitely needed for stationary and portable applications in the hydrogen-delivery infrastructure.

In this context, the conversion of H_2 with CO_2 to formic acid (HCOOH) merits special attention because HCOOH is a liquid that is easy to store and carry. In addition, HCOOH is a valuable raw material in organic syntheses and also an important intermediate in the water gas shift reaction.[80–82] If H_2 is readily converted with CO_2 to HCOOH, which can also be converted back to H_2 whenever H_2 is needed, HCOOH can be regarded as a liquid form of H_2 that is combined with CO_2.

The two-electron reduction of CO_2 generally results in the formation of formic acid and/or CO [reactions (1) and (3) in Scheme 11].[82,83] HCOOH is obtained by CO_2 insertion into the metal–H bond of a metal hydride complex to yield a metal formate complex, followed by intramolecular elimination of formic acid. The reverse process of reaction (1) in Scheme 11 is decarboxylation of HCOOH to produce CO_2 and H_2.[82] On the other hand, CO is obtained through the binding of CO_2 with a low-valent metal complex to form a metal–carbon bond, in which CO_2 is in the form of CO_2^{2-}, followed by protonation to yield CO and H_2O. The reverse process of reaction (2) in Scheme 11 is dehydration of HCOOH to produce CO and H_2O.[82] This

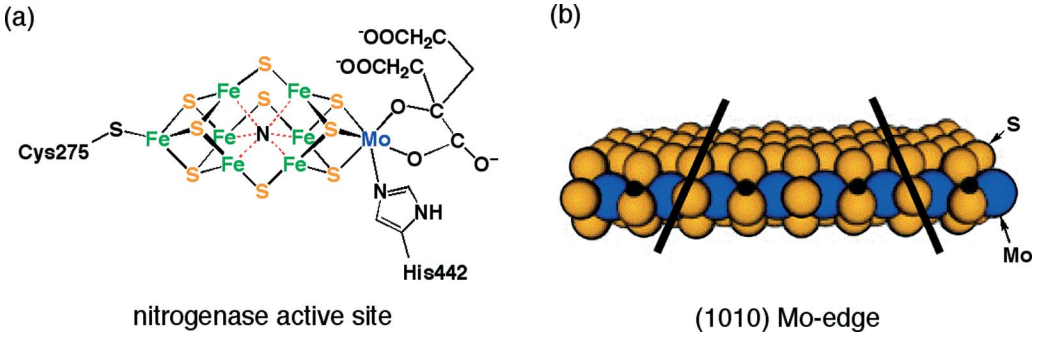

Figure 6. (a) Nitrogenase [FeMo] cofactor (FeMoco) with three hydrogen atoms bound at the equatorial 2S atoms.[72] (b) MoS_2 slab with the sulfur monomers present at the Mo edge.[73] The lines mark the dimension of the unit cell in the *x* direction.

is the dominant reaction in the gas phase, in the absence of catalysts.[84,85] Both types of reactions of HCOOH have been extensively investigated in gas phase, on the surface of metals, and in the homogeneous phase with metal complexes.[86–90] Reaction (3) is the widely studied "water gas shift" process, which provides a way of producing hydrogen gas through the use of transition-metal catalysts.[91–93] In most cases, both the decarboxylation and dehydration of HCOOH occur to produce a mixture of H_2 and CO. In order to use HCOOH as a liquid form of H_2 that is combined with CO_2, we need to have efficient catalysts for selective interconversion between H_2 and HCOOH [reaction (1) in Scheme 11].

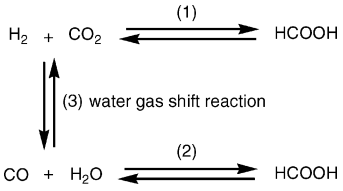

Scheme 11. Two-electron reduction of CO_2 with H_2 to afford (1) HCOOH or (3) CO and H_2O, and (3) water gas shift reaction.

From the view point of thermodynamics, it is desirable to use water as the solvent for interconversion between H_2 and HCOOH, because when all the reactants and the product are hydrated, the standard free energy is nearly zero (–4 kJ mol^{-1} at 298 K), whereas the reaction between gaseous H_2 and CO_2 yielding liquid HCOOH is accompanied by a free energy change of +33 kJ mol^{-1}.[82,83] The presence of bases in an aqueous solution of HCOOH makes the hydrogenation of CO_2 even more favorable.[82,83] Homogeneous catalysis in aqueous solutions requires water-soluble catalysts.

In aqueous solutions, the CO_2/hydrogen carbonate/carbonate equilibrium exists [Equation (1)].[80,83] Through this equilibrium the actual reactive species may change with changes in the pH, temperature, and CO_2 pressure. In aqueous systems, the addition of excess base is usually required for the catalytic hydrogenation of CO_2 and hydrogen carbonate with rhodium- and ruthenium-based complexes that have water-soluble phosphane ligands to afford the formate.[94,95] In such a case, separation of the base from the reaction medium is needed to obtain HCOOH.

$$CO_2 + H_2O \rightleftarrows HCO_3^- + H^+ \rightleftarrows CO_3^{2-} + 2H^+ \quad (1)$$

In contrast to ruthenium(II) complexes with water-soluble phosphane ligands, a water-soluble hydride complex $[Ru^{II}(bpy)(\eta^6\text{-}C_6Me_6)(H)]^+$ serves as a robust reducing agent for the reduction of CO_2 without involving hydrogen carbonate or carbonate under acidic conditions in a pH range of about 3–5 at ambient temperature to afford HCOOH selectively.[96] The hydride complex was synthesized from the reaction of an aqua complex $[Ru^{II}(bpy)(\eta^6\text{-}C_6Me_6)(OH_2)](SO_4)$ with $NaBH_4$ as a hydrogen donor in H_2O at about pH 7 at 25 °C. The X-ray analysis of the crystal shows that $[Ru^{II}(bpy)(\eta^6\text{-}C_6Me_6)(H)](CF_3SO_3)$ (Figure 7) adopts a distorted octahedral coordination geometry, and Ru^{II} is surrounded by one 6-C_6Me_6 ligand, one bpy ligand, and one terminal hydrido ligand. The IR spectrum shows a peak at 1908 cm^{-1} assigned to the Ru–H stretching mode that shifts to 1370 cm^{-1} by isotopic substitution of H by D.[96]

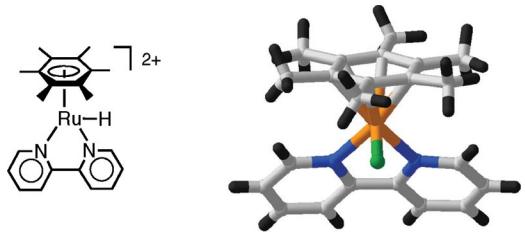

Figure 7. The X-ray structure of $[Ru^{II}(bpy)(\eta^6\text{-}C_6Me_6)(H)](CF_3SO_3)$.[96]

The rate of CO_2 reduction by the [Ru–H] complex increases linearly with increasing concentration of proton in the CO_2-saturated solution at 25 °C.[96] At pH 8.5, where HCO_3^- is the major species, the rate is 46 times smaller than that at pH 4.2, where CO_2 is the dominant species.[96] The mechanism for such an acid-catalyzed reduction of CO_2 with the [Ru–H] complex under acidic conditions is shown in Scheme 12.[96] It is interesting to note that an inverse kinetic isotope effect (k_H/k_D = 0.59) is observed for the reduction of CO_2 by the [Ru–H] complex.[96] Such inverse kinetic isotope effects were anticipated by Bigeleisen[97] for reactions in which the transition state has higher force constants than those for the ground state.[98,99] The force constants for the stretching (and bending) vibrations are significantly higher for C–H than for Ru–H bonds. Consequently, the difference in zero-point energy for Ru–H versus Ru–D is less than that for C–H versus C–D, which leads to the inverse kinetic isotope effect. Thus, the transition state may be sufficiently product-like (larger degree of C–H bond formation and correspondingly more M–H bond rupture) for the reduction of CO_2 by the [Ru–H] complex (Scheme 12).

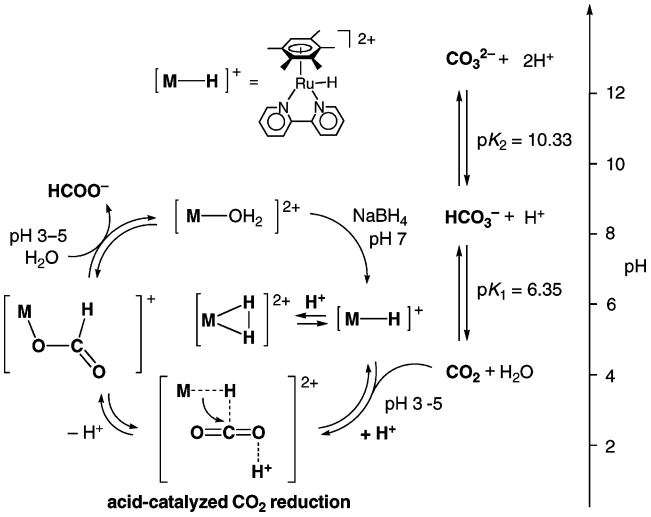

Scheme 12. Mechanism for the acid-catalyzed reduction of CO_2 to HCOOH with a [Ru–H] complex, $[Ru^{II}(bpy)(\eta^6\text{-}C_6Me_6)(H)]^+$.[96]

The aqua complexes, $[Ru^{II}(bpy)(\eta^6\text{-}C_6Me_6)(OH_2)](SO_4)$, $[Ru^{II}(\eta^6\text{-}C_6Me_6)(OH_2)(4,4'\text{-OMe-bpy})]SO_4$ (4,4′-OMe-bpy = 4,4′-dimethoxy-2,2′-bipyridine), and $[Ir^{III}Cp^*(L)(OH_2)]^{2+}$ ($Cp^* = \eta^5\text{-}C_5Me_5$, L = bpy and 4,4′-OMe-bpy) react with H_2 (5.5 MPa) and CO_2 (2.5 MPa) under acidic conditions (pH 3.0) in H_2O without base to catalytically provide HCOOH (Scheme 13).[100,101] The turnover numbers (TONs) of the aqueous hydrogenation of CO_2 catalyzed by $[Ru^{II}(bpy)(\eta^6\text{-}C_6Me_6)(OH_2)](SO_4)$ and $[Ru^{II}(\eta^6\text{-}C_6Me_6)(OH_2)(4,4'\text{-OMe-bpy})]SO_4$ at 40 °C after 70 h are 35 and 55, respectively.[100] The catalytic cycle for the aqueous hydrogenation of CO_2 with the ruthenium and iridium complexes under acidic conditions (pH 2.5–5.0) is shown in Scheme 13. The [Ru–H] and [Ir–H] complexes are generated by reaction of the aqua complexes with H_2 at pH 2.5–5.0.[100,101] The H_2O ligand accelerates heterolytic H_2 activation in polar solvents to release H_3O^+. The [Ru–H] and [Ir–H] complexes then react with CO_2 to afford the formate complex (the X-ray structure of the [Ru–formate] complex is shown in Scheme 13).[100,101] The TON over 12 h increases with increasing temperature to reach a maximum value at 40 °C and then decreases with a further increase in temperature.[100]

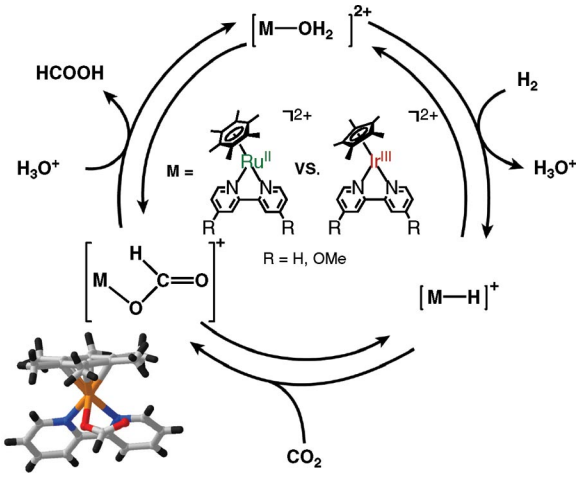

Scheme 13. Catalytic CO_2 reduction with H_2 to HCOOH and the back reaction with the evolution of hydrogen from ethanol with $[Ru^{II}(bpy)(\eta^6\text{-}C_6Me_6)(OH_2)]^+$ and $[Ir^{III}(bpy)Cp^*(OH_2)]^{2+}$ in an aqueous solution.[100,101] The X-ray crystal structure of the [Ru–formate] complex is also shown.

The backward reaction in Scheme 13 occurs at a higher temperature, which is attributed to a decrease in the TON, i.e. the reaction of $[Ru^{II}(\eta^6\text{-}C_6Me_6)(OH_2)(4,4'\text{-OMe-bpy})]SO_4$ with 10 equiv. HCOOH in H_2O at pH 2.4 at 60 °C was examined, and the disappearance of HCOOH (> 90%), together with evolution of H_2 and CO_2, was confirmed after 1 h by ^1H NMR spectroscopy and GC.[100] Thus, the direction of the reaction (the reduction of CO_2 with H_2 to HCOOH versus the decomposition of HCOOH back to CO_2 and H_2) can be controlled by temperature.

By applying the steady-state approximation to the active hydride species in Scheme 13, the rate of hydrogenation of CO_2, d[HCOOH]/dt, is expressed as a function of P_{H_2} and P_{CO_2}, as seen in Equation (2), where k_1 is the rate constant of the reaction of the aqua complex with H_2, k_{-1} is the rate constant of the back reaction, k_2 is the rate constant of the reaction of the hydride complex with CO_2, and $[\{M–OH_2\}^{2+}]_0$ is the initial concentration of the ruthenium or iridium aqua complex.

$$d[HCOOH]/dt = k_1k_2[\{Ru–OH_2\}^{2+}]_0P_{H_2}P_{CO_2}/(k_{-1} + k_1P_{H_2} + k_2P_{CO_2}) \quad (2)$$

Under conditions such that $k_{-1} >> k_1P_{H_2}$, Equation (2) is reduced to Equation (3), where the rate increases linearly with increasing P_{H_2} but exhibits saturation behavior with respect to increasing P_{CO_2}.

$$d[HCOOH]/dt = k_1k_2[\{Ru–OH_2\}^{2+}]P_{H_2}P_{CO_2}/(k_{-1} + k_2P_{CO_2}) \quad (3)$$

This was experimentally observed in the case of $[Ru^{II}(bpy)(\eta^6\text{-}C_6Me_6)(OH_2)]^{2+}$ as shown in Figure 8, where the TONs obtained in 3 h are used as an indication of the rate.[101] In such a case, the rate-determining step in the catalytic hydrogenation of CO_2 with the ruthenium catalysts is the reaction of the aqua complex with H_2, when the active hydride catalysts cannot be observed during the reaction.[101]

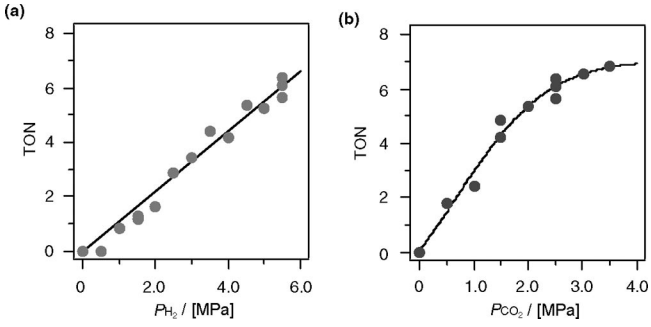

Figure 8. (a) H_2-pressure-dependent TONs for the hydrogenation of CO_2 catalyzed by $[Ru^{II}(\eta^6\text{-}C_6Me_6)(OH_2)(4,4'\text{-OMe-bpy})]SO_4$ (20.0 μmol) at pH 3.0 in a citrate buffer solution (20 cm^3) at 40 °C for 3 h at 2.5 MPa of CO_2.[101] (b) CO_2-pressure-dependent TONs for the hydrogenation of CO_2 catalyzed by the Ru complex (20.0 μmol) at pH 3.0 in a citrate buffer solution (20 cm^3) at 40 °C for 3 h at 5.5 MPa of H_2.[101]

In contrast to the case of the ruthenium complexes, the active hydride catalysts, $[Ir^{III}Cp^*(H)(L)]^+$ (L = bpy and 4,4′-OMe-bpy) have successfully been isolated after the hydrogenation of CO_2 with the iridium complexes.[101] The ^1H NMR spectrum of $[Ir^{III}Cp^*(H)(4,4'\text{-OMe-bpy})]^+$ in $[D_6]$-DMSO exhibits a characteristic signal of the hydride ligand at –11.25 ppm.[101] In this case, the rate-determining step changes from the reaction of the $[M–OH_2]$ complex with H_2 to the reaction of the [Ir–H] complex with CO_2. The

TON increases linearly with increasing P_{CO_2} but exhibits saturation behavior with respect to increasing P_{H_2} [Equation (4) and Figure 9].[101]

$$d[HCOOH]/dt = k_1k_2[\{Ir–OH_2\}^{2+}]P_{CO_2}P_{H_2}/(k_{-1} + k_1P_{H_2}) \quad (4)$$

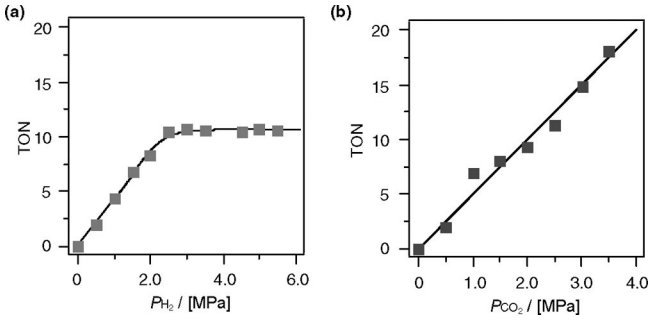

Figure 9. (a) H_2-pressure-dependent TONs for the hydrogenation of CO_2 catalyzed by $[Ir^{III}Cp^*(OH_2)(4,4'\text{-OMe-bpy})]SO_4$ (20.0 μmol) at pH 3.0 in a citrate buffer solution (20 cm^3) at 40 °C for 0.5 h at 2.5 MPa of CO_2.[101] (b) CO_2-pressure-dependent TONs for the hydrogenation of CO_2 catalyzed by the Ir complex at pH 3.0 in a citrate buffer solution (20 cm^3) at 40 °C for 0.5 h at 5.5 MPa of H_2.[101]

The IR spectra of the [Ir–H] and [Ru–H] complexes indicate that the strength of the Ir–H bonds is higher than that of the Ru–H bonds.[101] This may be the reason for the difference in the rate-determining steps between hydrogenation with the iridium complexes and that with the ruthenium complexes. The catalytic activity of iridium catalysts is also higher than that of the ruthenium catalysts. The initial TOF (2.0 h^{-1}) of the [Ir–OH_2] complex with the bpy ligand ($[Ir^{III}(bpy)Cp^*(OH_2)]^{2+}$) under the conditions of P_{H_2}/P_{CO_2} = 5.5/2.5 MPa at pH 3.0 in a citrate buffer solution at 40 °C significantly improves by introducing an electron-donating substituent on the ligand of the iridium complex ($[Ir^{III}Cp^*(OH_2)(4,4'\text{-OMe-bpy})]^{2+}$) up to 27 h^{-1}, which is more than 100 times faster than that observed for the [Ru–OH_2] complex with the bpy ligand.[101] Such an electronic substituent effect in a bipyridine ligand has generally been observed for the catalytic hydrogenation of CO_2.[95,102]

A Rh complex [Rh(bpy)(Cl)Cp*]Cl has also been reported to be effective for the hydrogenation of CO_2 in aqueous solution.[103] Since the interconversion between H_2 and HCOOH is thermodynamically reversible (vide supra), a proper choice of metal and ligand may be essential for obtaining a highly efficient catalytic activity for the decomposition of HCOOH back to H_2 and CO_2, as well as for the hydrogenation of CO_2 to HCOOH.[95,104]

Conclusions

In summary, a simplified model of the photosynthesis reaction center (Acr^+–Mes) has been used to develop a highly efficient photocatalytic hydrogen-evolution system *without an electron mediator* such as MV^{2+}, which is composed of Acr^+–Mes, NADH, and a water-soluble platinum colloid to achieve the highest quantum yield for hydrogen production (26 ± 3%) ever reported. NADH is replaced by ethanol as an electron source in the presence of ADH for the catalytic evolution of hydrogen. The next goal will be the construction of an efficient catalytic system for the evolution of hydrogen from water without a sacrificial electron donor by using solar energy, where the development of an efficient water oxidation catalyst remains a formidable challenge. Once hydrogen is produced, hydrogen can be stored, by combining with CO_2, in the form of HCOOH, which is easy to store and carry. Some efficient catalytic systems are now available for the catalytic interconversion between H_2 and HCOOH in aqueous solution. Hybrid systems that combine the advantages of homogeneous and heterogeneous catalysts as well as enzymes merit considerable attention for the future development of more efficient photocatalytic generation of H_2 and storage. These systems will certainly contribute to finding optimum solutions to global energy and environmental issues in the 21st century.

Acknowledgments

The author gratefully acknowledges the contributions of his collaborators and co-workers, in particular Prof. Hiroshi Imahori, Prof. Seiji Ogo, Dr. Kei Ohkubo, and Dr. Hiroaki Kotani, mentioned in the cited references. The author thanks the Ministry of Education, Culture, Sports, Science and Technology, Japan, for continuous support. The financial support to our PhD students by the Global COE program, "The Global Education and Research Center for Bio-Environmental Chemistry" is also gratefully acknowledged.

[1] D. L. Royer, R. A. Berner, J. Park, *Nature* **2007**, *446*, 530–532.
[2] N. S. Lewis, D. G. Nocera, *Proc. Natl. Acad. Sci. USA* **2006**, *103*, 15729–15735.
[3] R. A. Kerr, R. F. Service, *Science* **2005**, *309*, 101.
[4] S. Z. Baykara, *Int. J. Hydrogen Energy* **2005**, *30*, 545–553.
[5] R. E. Blankenship, M. T. Madigan, C. E. Bauer (Eds.), *Anoxygenic Photosynthetic Bacteria*, Kluwer, Dordrecht, **1995**.
[6] D. Gust, T. A. Moore, A. L. Moore in *Electron Transfer in Chemistry* (Ed.: V. Balzani), Wiley-VCH, Weinheim, **2001**, vol. 3, pp. 272–336.
[7] D. Gust, T. A. Moore, A. L. Moore, *Acc. Chem. Res.* **2001**, *34*, 40–48.
[8] K. D. Jordan, M. N. Paddon-Row, *Chem. Rev.* **1992**, *92*, 395–410.
[9] M. N. Paddon-Row, *Adv. Phys. Org. Chem.* **2003**, *38*, 1–85.
[10] M. R. Wasielewski, *Chem. Rev.* **1992**, *92*, 435–461.
[11] J. W. Verhoeven, *Adv. Chem. Phys.* **1999**, *106*, 603–644.
[12] A. Harriman, J.-P. Sauvage, *Chem. Soc. Rev.* **1996**, *25*, 41–48.
[13] S. Fukuzumi, H. Imahori in *Electron Transfer in Chemistry* (Ed.: V. Balzani), Wiley-VCH, Weinheim, **2001**, vol. 2, pp. 927–975.
[14] D. M. Guldi, M. Prato, *Acc. Chem. Res.* **2000**, *33*, 695–703.
[15] D. M. Guldi, G. M. A. Rahman, V. Sgobba, C. Ehli, *Chem. Soc. Rev.* **2006**, *35*, 471–487.
[16] S. Fukuzumi, D. M. Guldi in *Electron Transfer in Chemistry* (Ed.: V. Balzani), Wiley-VCH, Weinheim, **2001**, vol. 2, pp. 270–337.
[17] S. Fukuzumi, *Org. Biomol. Chem.* **2003**, *1*, 609–620.
[18] S. Fukuzumi, *Functional Organic Materials*, Wiley-VCH, **2007**, pp. 465–510.
[19] J.-M. Lehn, J.-P. Sauvage, *Nouv. J. Chim.* **1977**, *1*, 449–451.
[20] K. Kalyanasundaram, *Coord. Chem. Rev.* **1982**, *46*, 159–244.
[21] J. R. Darwent, P. Douglas, A. Harriman, G. Porter, M.-C. Richoux, *Coord. Chem. Rev.* **1982**, *44*, 83–126.

[22] C. Laane, I. Willner, J. W. Otvos, M. Calvin, *Proc. Natl. Acad. Sci. USA USA.* **1981**, *78*, 5928.
[23] M. Grätzel, *Acc. Chem. Res.* **1981**, *14*, 376–384.
[24] S.-F. Chan, M. Chou, C. Creutz, T. Matsubara, N. Sutin, *J. Am. Chem. Soc.* **1981**, *103*, 369–379.
[25] C. V. Krishnan, B. S. Brunschwig, C. Creutz, N. Sutin, *J. Am. Chem. Soc.* **1985**, *107*, 2005–2015.
[26] P. Du, J. Schneider, P. Jarosz, R. Eisenberg, *J. Am. Chem. Soc.* **2006**, *128*, 7726–7727.
[27] E. H. Yonemoto, R. L. Riley, Y. I. Kim, S. J. Atherton, R. H. Schmehl, T. E. Mallouk, *J. Am. Chem. Soc.* **1992**, *114*, 8081–8087.
[28] N. Toshima, K. Hirakawa, *Polym. J.* **1999**, *31*, 1127–1132.
[29] I. Okura, N. Kim-Thuan, *J. Mol. Catal.* **1979**, *6*, 227–230.
[30] I. Okura, *Coord. Chem. Rev.* **1985**, *68*, 53–99.
[31] Y. Amao, Y. Tomonou, I. Okura, *Solar Energy Mater. Solar Cells* **2003**, *79*, 103–111.
[32] I. Okura, H. Hosono, *J. Phys. Chem.* **1992**, *96*, 4466–4469.
[33] L. Persaud, A. J. Bard, A. Campion, M. A. Fox, T. E. Mallouk, S. E. Webber, J. M. White, *J. Am. Chem. Soc.* **1987**, *109*, 7309–7314.
[34] D.-L. Jiang, C.-K. Choi, K. Honda, W.-S. Li, T. Yuzawa, T. Aida, *J. Am. Chem. Soc.* **2004**, *126*, 12084–12089.
[35] H. Imahori, K. Tamaki, D. M. Guldi, C. Luo, M. Fujitsuka, O. Ito, Y. Sakata, S. Fukuzumi, *J. Am. Chem. Soc.* **2001**, *123*, 2607–2617.
[36] S. Fukuzumi, S. Koumitsu, K. Hironaka, T. Tanaka, *J. Am. Chem. Soc.* **1987**, *109*, 305–316.
[37] S. Fukuzumi, H. Imahori, K. Okamoto, H. Yamada, M. Fujitsuka, O. Ito, D. M. Guldi, *J. Phys. Chem. A* **2002**, *106*, 1903–1908.
[38] H. Imahori, M. Arimura, T. Hanada, Y. Nishimura, I. Yamazaki, Y. Sakata, S. Fukuzumi, *J. Am. Chem. Soc.* **2001**, *123*, 335–336.
[39] A. P. Alivisatos, *Science* **1996**, *271*, 933–937.
[40] P. V. Kamat, *J. Phys. Chem. B* **2002**, *106*, 7729–7744.
[41] S. Fukuzumi, Y. Endo, H. Imahori, Y. Araki, O. Ito, *J. Phys. Chem. B* **2003**, *107*, 11979–11986.
[42] H. Kotani, K. Ohkubo, Y. Takai, S. Fukuzumi, *J. Phys. Chem. B* **2006**, *110*, 24047–24053.
[43] A. C. Templeton, D. E. Cliffel, R. W. Murray, *J. Am. Chem. Soc.* **1999**, *121*, 7081–7089.
[44] H. Imahori, Y. Kashiwagi, T. Hanada, Y. Endo, Y. Nishimura, I. Yamazaki, S. Fukuzumi, *J. Mater. Chem.* **2003**, *13*, 2890–2898.
[45] S. E. Eklund, D. E. Cliffel, *Langmuir* **2004**, *20*, 6012–6018.
[46] Y. Li, J. Petroski, M. A. El-Sayed, *J. Phys. Chem. B* **2000**, *104*, 10956–10959.
[47] S. Fukuzumi, H. Kotani, K. Ohkubo, S. Ogo, N. V. Tkachenko, H. Lemmetyinen, *J. Am. Chem. Soc.* **2004**, *126*, 1600–1601.
[48] K. Ohkubo, H. Kotani, S. Fukuzumi, *Chem. Commun.* **2005**, 4520–4522.
[49] H. Kotani, K. Ohkubo, S. Fukuzumi, *J. Am. Chem. Soc.* **2004**, *126*, 15999–16006.
[50] X.-Q. Zhu, Y. Yang, M. Zhang, J.-P. Cheng, *J. Am. Chem. Soc.* **2003**, *125*, 15298–15299.
[51] S. Fukuzumi, T. Tanaka in *Photoinduced Electron Transfer* (Eds.: M. A. Fox, M. Chanon), Elsevier, Amsterdam, **1988**, part C, pp. 578–635.
[52] H. Kotani, T. Ono, K. Ohkubo, S. Fukuzumi, *Phys. Chem. Chem. Phys.* **2007**, *9*, 1487–1492.
[53] S. Özkar, R. G. Finke, *J. Am. Chem. Soc.* **2002**, *124*, 5796–5810.
[54] L. Qiu, F. Liu, L. Zhao, W. Yang, J. Yao, *Langmuir* **2006**, *22*, 4480–4482.
[55] J. Handman, A. Harriman, G. Porter, *Nature* **1984**, *307*, 534.
[56] H. Ozawa, M. Haga, K. Sakai, *J. Am. Chem. Soc.* **2006**, *128*, 4926–4927.
[57] C. D. Ellis, L. D. Margerum, R. W. Murray, T. J. Meyer, *Inorg. Chem.* **1983**, *22*, 1283–1291.
[58] Y. Astuti, E. Palomares, S. A. Haque, J. R. Durrant, *J. Am. Chem. Soc.* **2005**, *127*, 15120–15126.
[59] H. G. Kim, D. W. Hwang, J. Kim, Y. G. Kim, J. S. Lee, *Chem. Commun.* **1999**, 1077–1078.
[60] G. K. Mor, K. Shankar, M. Paulose, O. K. Varghese, C. A. Grimes, *Nano Lett.* **2005**, *5*, 191–195.
[61] M. W. W. Adams, E. I. Stiefel, *Science* **1998**, *282*, 1842–1843.
[62] A. L. De Lacey, V. M. Fernandez, M. Rousset, R. Cammack, *Chem. Rev.* **2007**, *107*, 4304–4330.
[63] A. Volbeda, M.-H. Charon, C. Piras, E. C. Hatchikian, M. Frey, J. C. Fontecilla-Camps, *Nature* **1995**, *373*, 580–587.
[64] S. E. Lamle, S. P. J. Albracht, F. A. Armstrong, *J. Am. Chem. Soc.* **2005**, *127*, 6595–6604.
[65] C. Tard, X. Liu, S. K. Ibrahim, M. Bruschi, L. De Gioia, S. C. Davies, X. Yang, L.-S. Wang, G. Sawers, C. J. Pickett, *Nature* **2005**, *433*, 610–613.
[66] P. Liu, J. A. Rodriguez, *J. Am. Chem. Soc.* **2005**, *127*, 14871–14878.
[67] T. Abura, S. Ogo, Y. Watanabe, S. Fukuzumi, *J. Am. Chem. Soc.* **2003**, *125*, 4149–4154.
[68] C. J. Curtis, A. Miedaner, W. W. Ellis, D. L. DuBois, *J. Am. Chem. Soc.* **2002**, *124*, 1918–1925.
[69] A. Volbeda, M.-H. Charon, C. Piras, E. C. Hatchikian, M. Frey, J.-C. Fontecilla-Camps, *Nature* **1995**, *373*, 580–587.
[70] A. Volbeda, E. Garcin, C. Piras, A. L. de Lacey, V. M. Fernandez, E. C. Hatchikian, M. Frey, J.-C. Fontecilla-Camps, *J. Am. Chem. Soc.* **1996**, *118*, 12989–12996.
[71] S. Ogo, R. Kabe, K. Uehara, B. Kure, T. Nishimura, S. C. Menon, R. Harada, S. Fukuzumi, Y. Higuchi, T. Ohhara, T. Tamada, R. Kuroki, *Science* **2007**, *316*, 585–587.
[72] M. Carepo, D. L. Tierney, C. D. Brondino, T. C. Yang, A. Pamplona, J. Telser, J. J. G. Moura, B. M. Hoffman, *J. Am. Chem. Soc.* **2002**, *124*, 281–286.
[73] M. Brecht, M. van Gaster, T. Buhrke, B. Friedrich, W. Lubitz, *J. Am. Chem. Soc.* **2003**, *125*, 13075–13083.
[74] P. E. M. Siegbahn, *Adv. Inorg. Chem.* **2004**, *56*, 101.
[75] B. Hinnemann, P. G. Moses, J. Bonde, K. P. Jøensen, J. H. Nielsen, S. Horch, I. Chokrendorff, J. K. Nørskov, *J. Am. Chem. Soc.* **2005**, *127*, 5308–5309.
[76] P. Raybaud, J. Hafner, G. Kresse, S. Kasztelan, H. Toulhoat, *J. Catal.* **2000**, *189*, 129.
[77] T. F. Jaramillo, K. P. Jøgensen, J. Bonde, J. H. Nielsen, S. Horch, I. Chokendorff, *Science* **2007**, *317*, 100–102.
[78] R. F. Service, *Science* **2004**, *305*, 958–961.
[79] R. Cammack, M. Frey, R. Robson, *Hydrogen as a Fuel: Learning from Nature*, Taylor & Francis, London, **2001**.
[80] P. G. Jessop, T. Ikariya, R. Noyori, *Chem. Rev.* **1995**, *95*, 259–272.
[81] W. Leitner, *Angew. Chem. Int. Ed. Engl.* **1995**, *34*, 2207–2221.
[82] P. G. Jessop, F. Joó, C.-C. Tai, *Coord. Chem. Rev.* **2004**, *248*, 2425–2442.
[83] P. G. Jessop in *Handbook of Homogeneous Hydrogenation*, Vol. 1 (Eds. J. G. De Vries, C. J. Elsevier), Wiley-VCH, Weinheim, **2007**, pp. 489–511.
[84] K. Saito, T. Kakumoto, H. Kuroda, S. Torii, A. Imamura, *J. Chem. Phys.* **1984**, *80*, 4989–4996.
[85] K. Saito, T. Shiose, O. Takahashi, Y. Hidaka, F. Aiba, K. Tabayashi, *J. Phys. Chem. A* **2005**, *109*, 5352–5357.
[86] M. Arenz, V. Stamenkovic, P. N. Ross, N. M. Markovic, *Surf. Sci.* **2004**, *573*, 57–66.
[87] M. Arenz, V. Stamenkovic, T. J. Schmidt, K. Wandelt, P. N. Ross, N. M. Markovic, *Phys. Chem. Chem. Phys.* **2003**, *5*, 4242–4251.
[88] C. Xu, D. W. Goodman, *J. Phys. Chem.* **1996**, *100*, 1753–1760.
[89] J. B. Fenn, M. Mann, C. K. Meng, S. F. Wong, C. M. Whitehouse, *Science* **1989**, *246*, 64–71.
[90] P. Chen, *Angew. Chem. Int. Ed.* **2003**, *42*, 2832–2847.
[91] Q. Fu, H. Saltsburg, M. Flytzani-Stephanopoulos, *Science* **2003**, *301*, 935–938.

[92] C. V. Ovesen, P. Stoltze, J. K. Norskov, C. T. Campbell, *J. Catal.* **1992**, *134*, 445–468.
[93] J. Knudsen, A. U. Nilekar, R. T. Vang, J. Schnadt, E. L. Kunkes, J. A. Dumesic, M. Mavrikakis, F. Besenbache, *J. Am. Chem. Soc.* **2007**, *129*, 6485–6490.
[94] G. Laurenczy, F. Joo, L. Nadasdi, *Inorg. Chem.* **2000**, *39*, 5083–5088.
[95] Y. Himeda, *Eur. J. Inorg. Chem.* **2007**, 3927–3941.
[96] H. Hayashi, S. Ogo, T. Abura, S. Fukuzumi, *J. Am. Chem. Soc.* **2003**, *125*, 14266–14267.
[97] J. Bigeleisen, *J. Chem. Phys.* **1949**, *17*, 675–678.
[98] J. Bigeleisen, *Pure Appl. Chem.* **1964**, *8*, 217–223.
[99] T.-Y. Cheng, R. M. Bullock, *J. Am. Chem. Soc.* **1999**, *121*, 3150–3155.
[100] H. Hayashi, S. Ogo, S. Fukuzumi, *Chem. Commun.* **2004**, 1714–1715.
[101] S. Ogo, R. Kabe, H. Hayashi, R. Harada, S. Fukuzumi, *Dalton Trans.* **2006**, 4657–4663.
[102] C. C. Tai, J. Pitts, J. C. Linehan, A. D. Main, P. Munshi, P. G. Jessop, *Inorg. Chem.* **2002**, *41*, 1606.
[103] Y. Himeda, N. Onozawa-Komatsuzaki, H. Sugihara, H. Arakawa, K. Kasuga, Japan Patent 3968431, **2007**.
[104] Y. Himeda, N. Onozawa-Komatsuzaki, H. Sugihara, H. Arakawa, K. Kasuga, *Organometallics* **2004**, *23*, 1480–1483.

Received: December 27, 2007
Published Online: February 20, 2008

